Hindawi
Structural Control and Health Monitoring
Volume 2024, Article ID 3271106, 21 pages
https://doi.org/10.1155/2024/3271106

Research Article

Condition Monitoring and Quantitative Evaluation of Railway Bridge Substructures Using Vehicle-Induced Vibration Responses by Sparse Measurement

Chuang Wang, Jiawang Zhan, Yujie Wang, Xinxiang Xu, and Zhihang Wang

School of Civil Engineering, Beijing Jiaotong University, Beijing 100044, China

Correspondence should be addressed to Jiawang Zhan; jwzhan@bjtu.edu.cn

Received 13 November 2023; Revised 19 January 2024; Accepted 21 March 2024; Published 2 April 2024

Academic Editor: Zoran Rakicevic

Bridge substructure failure has been responsible for numerous recorded bridge collapses, particularly for small- and medium-span bridges, so it is crucial to effectively monitor the performance of the bridge substructures for efficient maintenance and management. The current vibration-based approaches for quantitatively evaluating bridge substructures rely on in-situ experiments with a multitude of sensors or impact vibration test, making it challenging to implement long-term online monitoring. This paper proposes an accurate, low cost, and practicable method to achieve online quantitative monitoring of railway bridge substructures using only one vibration sensor and operational train-induced vibration responses. The newly derived flexible-base Timoshenko beam models, along with the random decrement technique and Levenberg–Marquardt–Fletcher algorithm, are employed to identify the modal parameters and quantitatively assess the condition of bridge substructures. The proposed method is numerically verified through an established 3D train-bridge-foundation coupling system considering different damage scenarios. In addition, a real-world application is also conducted on the 2nd Songhua River bridge in the Harbin–Dalian high-speed railway, aiming at examining the effectiveness and robustness of the method in condition monitoring of bridge substructure under a complete freeze-thaw cycle. The results indicate that the proposed methodology is effective in extracting the modal parameters and monitoring the state evolution of the bridge substructures, which offers an efficient and accurate strategy for condition monitoring and quantitative evaluation of railway bridge substructures.

1. Introduction

The safety and reliability assessment of bridges is essential to ensure the smooth functioning of railways. Currently, there are approximately 92,000 railway bridges in China, including over 30,000 high-speed railway (HSR) bridges. However, several of these bridges have been in service for a substantial period, which increases the potential for uncertainty regarding their serviceability [1]. Furthermore, newer bridges may experience a decline in service performance as a result of intricate external actions, such as train dynamic load, flood erosion, debris flow, freeze-thaw cycles, vehicle collisions, and earthquakes. Consequently, railway bridge substructures are susceptible to various defects, including foundation settlement, pier tilting, and pier corrosion, leading to issues such as foundation damage, lower structural stiffness, reduced durability, and insufficient bearing capacity. It is worth noting that a lot of bridge collapses can be attributed to the substructure failures [2, 3]. Therefore, there is an urgent requirement to evaluate and continuously monitor the service status of a vast number of bridge substructures.

Damages affecting the bridge substructures normally under the surface of ground or water, possessing high degrees of invisibility and suddenness. As such, they are challenging to detect and evaluate merely through visual inspections. To address this issue, many approaches have been explored to assess the condition of bridge substructures. Conventional inspection approaches, such as excavation and coring, are the simplest and most efficient methods, regardless of the foundation type, but at the same time they may affect the integrity and safety of the bridge

substructure and are economically incompatible. To avoid these problems, many nondestructive testing (NDT) techniques have been deeply examined on bridge substructures and foundations.

Hossain et al. [4] evaluated unknown foundation depth using different NDT methods. They proved that the parallel seismic (PS) method and resistivity imaging (RI) method were effective to evaluate the foundation depth. Chen et al. [5] leveraged sonar imaging technology to detect the underwater foundation damage of an ancient stone arch bridge. Rashidyan et al. [6] investigated the practicability of the Induction Field Testing in determining the depth of steel and reinforced concrete foundations. Cardoso and Lopes [7] demented that electrical resistivity tomography (ERT) could be used to assess the bridge foundation depth. However, the practicality of these techniques is limited and influenced by the characteristics of the substructure, soil characteristics, access restrictions, equipment costs, and experience of inspectors, and can only be used to determine the presence or absence of damage. Additionally, using buried sensors is a direct NDT approach to monitor bridge scour, such as the application of fiber Bragg grating sensors [8, 9], magnet-based smart rocks [10–12], and piezoelectric sensors [13]. Of note, these sensors for direct measurement are generally expensive and can only for one-time use, and the installation and replacement process are challenging.

An alternative approach, called vibration-based method, adopts changes in modal parameters and their derived indicators to assess structural conditions [14], which shows great potential for detecting concealed damage and evaluating the overall service performance of structures. Recently, many researchers have reported methods for scour detection based on natural frequencies and mode shapes [15–19], which can preliminarily detect the presence of damage. To further quantitatively characterize the bridge substructure, system identification methods in conjunction with analytical model are leveraged to obtain calibrated finite element model (FEM) or structural physical parameters.

Chen et al. [20] developed a foundation scour evaluation method using the ambient vibration measurements of the bridge superstructure, and the soil stiffness and scour depth were estimated from a globally best fitted finite element model. Davis and Sanayei [21] utilized live load dynamic strain and accelerations measured from substructure elements during operational loading to evaluate the bridge foundations. Mao et al. [22] employed experimental modal analysis and finite element model updating to estimate the unknown foundation depth and conditions of the bridge substructure. A scaled bridge model experiment was also conduced to better understand different factors affecting structural identification technique for substructure characterization [2]. Carbonari et al. [23] proposed a methodology for identifying physical parameters of soil-foundation-bridge pier systems from identified state-space models. Ghorbani et al. [3] developed an out-put only scour level quantification method by integrating an unscented Kalman filter, random decrement, and a continuous Euler–Bernoulli beam model. Zhan et al. [24] proposed a systematic procedure for HSR bridge substructure evaluation based on a simplified model and finite element model updating. They further used vibration measurements and finite element model updating to quantitatively evaluate the scour depth of highway bridge piers [25].

The abovementioned literatures demonstrate that the system identification methods can effectively localize and quantify the damage of bridge substructure. However, some of these methods require the application of impact loads and cannot be used for long-term online monitoring, and most approaches require the installation of many sensors, which can lead to difficulties in management and processing of massive data. This paper aims to develop an accurate, low-cost, and practicable method to achieve online quantitative monitoring of railway bridge substructures using sparse measurements and operational train-induced vibrations. A newly derived flexible-base Timoshenko beam models, along with the random decrement technique and Levenberg–Marquardt–Fletcher algorithm, are integrated to identify the modal parameters and quantitatively assess the condition of bridge substructures. In summary, the main contributions of the present study can be briefly itemized as follows: (1) presenting a flexible-base Timoshenko beam model for bridge substructure to accurately interpret the transverse dynamics of different types of bridge substructures; (2) proposing a methodology that can quantitatively evaluate the condition of railway bridge substructures using only one vibration sensor and operational train-induced vibration responses; and (3) validating the feasibility and effectiveness of the methodology in a real-world application using online monitoring data during a complete freeze-thaw cycle.

The paper is structured as follows: First, a 3D train-bridge-foundation coupling analytical model is established, which is suitable for interpreting the dynamics of the entire system. A flexible-base Timoshenko beam model is derived to characterize the transverse dynamics of the local pier-beam system, and the random decrement technique and Levenberg–Marquardt–Fletcher algorithm, are integrated to lead a novel framework for quantitatively assessing the condition of bridge substructures. Then, the effectiveness of the proposed methodology is numerically investigated via the 3D train-bridge interaction model, considering single damage, multiple damages, and varying pier heights. Finally, field tests that involve the impact vibration test and train-induced vibration test were conducted to verify the feasibility of the proposed modal analysis method for bridge substructures. Furthermore, monitoring of the bridge substructure during a complete freeze-thaw cycle was carried out to examine the effectiveness and robustness of the method in quantitatively monitoring the health condition of the bridge substructures.

2. Establishment of 3D Train-Bridge-Foundation Coupling System

The dynamic interaction of a train-bridge-foundation system is a complicated and coupled problem that varies with time. This type of issue is usually solved through numerical simulation methods by establishing a dynamic interaction

model for the train-bridge system. The analytical model can be regarded as a large spatial dynamic system consisting of two subsystems, namely, the train and bridge subsystems. Each subsystem can be simulated as an elastic structure with unique vibration patterns. The 3D HSR train-bridge-foundation system is depicted schematically in Figure 1.

2.1. Multibody Dynamic Model of Train. The train model is formulated based on the multi-body dynamic theory. A single train is composed of a car-body, two bogies and four wheel-sets, which are all assumed to be rigid and their elastic deformation during vibration are neglected. The primary and secondary suspension systems are characterized by liner springs and viscous dampers. The vibration of the car-body, bogie, and wheel-set along the longitudinal axis of the vehicle is not considered. Therefore, each car-body or bogie has 5 DOFs, namely, lateral displacements Y_{ci} and Y_{tij}, vertical displacements Z_{ci} and Z_{tij}, roll displacements θ_{ci} and θ_{tij}, pitch displacements φ_{ci} and φ_{tij} and yaw displacements ψ_{ci} and ψ_{tij}. The wheels-set has 3 DOFs in directions of Y_{wijl}, Z_{wijl}, θ_{wijl}, where i denotes the i^{th} vehicle, $j = 1, 2$ represent the front and rear bogies, and $l = 1, 2, 3, 4$ represent four wheel-sets, respectively. Therefore, the train model is established as a four-axle vehicle with 27 DOFs. The 8 marshaling trains pass over the bridge at a constant speed V, and the schematic view of HSR train is shown in Figure 2. The dynamic equation of the vehicle can be given as

$$\mathbf{M}_{\text{v}}\mathbf{x}_{\text{v}} + \mathbf{C}_{\text{v}}\dot{\mathbf{x}}_{\text{v}} + \mathbf{K}_{\text{v}}\mathbf{x}_{\text{v}} = \mathbf{F}_{\text{v}}, \tag{1}$$

where $\mathbf{M}_{\text{v}}$, $\mathbf{C}_{\text{v}}$, and $\mathbf{K}_{\text{v}}$ denote the mass, damping, and stiffness matrices of the train, respectively; $\mathbf{x}_v$, $\dot{\mathbf{x}}_v$, and $\mathbf{x}_v$ are the vector of train displacement, velocity, and acceleration, respectively.

2.2. Finite Element Model of Bridge. The HSR bridge is composed of tracks, girders, bearings, piers, and pile foundations, which is typically established by spatial FEM. It is assumed that there is no relative displacement between track and bridge deck, i.e. the elastic deformation of ballastless track system (including the fastener, track plate, base plate, and CA mortar layer) is neglected. The motion equations of the bridge subsystem can be expressed as

$$\mathbf{M}_{\text{b}}\mathbf{x}_{\text{b}} + \mathbf{C}_{\text{b}}\dot{\mathbf{x}}_{\text{b}} + \mathbf{K}_{\text{b}}\mathbf{x}_{\text{b}} = \mathbf{F}_{\text{b}}, \tag{2}$$

where $\mathbf{M}_b$, $\mathbf{C}_b$, $\mathbf{K}_b$ are the bridge global mass, damping, and stiffness matrices in order; $\mathbf{x}_b$, $\dot{\mathbf{x}}_b$, and $\mathbf{x}_b$ are the bridge displacement, velocity, and acceleration, respectively; $\mathbf{F}_b$ is the force acting on the bridge deck by the wheel-sets.

The equivalent stiffness matrix is introduced into the bridge model to consider the soil-structure interaction, and then the stiffness matrix can be given as

$$\widehat{\mathbf{K}}_{\text{b}} = \begin{bmatrix} \mathbf{K}_{\text{b}} & \mathbf{K}_{\text{bp}} \\ \mathbf{K}_{\text{pb}} & \mathbf{K}_{\text{b}} + \mathbf{K}_{\text{piles}} \end{bmatrix}, \tag{3}$$

where $\mathbf{K}_{\text{bp}}$ and $\mathbf{K}_{\text{pb}}$ are interaction stiffness submatrices between bridge piers and piles, respectively; $\mathbf{K}_{\text{piles}}$ is the equivalent stiffness matrix of group-piles determined by [26, 27], which mainly includes two procedures: determination of m (the scale coefficient of soil horizontal resistance) and calculation of equivalent stiffness coefficient of group-piles.

The damping matrix $\mathbf{C}_b$ adopts the Rayleigh damping expressed as follows [27]:

$$\mathbf{C}_{\text{b}} = \frac{2\xi\omega_1\omega_2}{\omega_1 + \omega_2}\mathbf{M}_{\text{b}} + \frac{2\xi}{\omega_1 + \omega_2}\mathbf{K}_{\text{b}} \tag{4}$$

where ξ is the bridge damping ratio; ω_1 and ω_2 are the first and second-order transverse circular frequencies of the bridge in order.

2.3. Wheel-Rail Interaction Relationship and Track Irregularity. Different wheel-rail contact models have their own superiorities. Since the overall responses of the train-bridge system are concerned in this study, the vertical wheel-rail correspondence assumption and lateral simplified Kalker linear creep theory are leveraged, which can provide sufficient calculation accuracy while do not need complicated analysis of wheel-rail contact geometry [27].

The wheel-rail correspondence model assumes no relative movement between the wheel and the rail in the Z-direction of vehicle coordinates. The displacements of the wheel-sets and the bridge couple together through the track irregularity with the following equations:

$$Z_{\text{w}i} = Z_{\text{b}}(x_{wi}) + Z_{\text{s}}(x_{wi}), \dot{Z}_{wi} = \dot{Z}_{\text{b}}(x_{wi}) + \dot{Z}_{\text{s}}(x_{wi}), \ddot{Z}_{\text{w}i} = \ddot{Z}_{\text{b}}(x_{\text{w}i}) + \ddot{Z}_{\text{s}}(x_{\text{w}i}), \tag{5}$$

where x_{wi} is the position of the i^{th} wheel-set ($i = 1, 2, 3, 4$); Z, $\dot{Z}$, $\ddot{Z}$ are the displacement, velocity and acceleration, respectively; subscripts "wi", "b", and "s" denote the wheel-set, the bridge, and the track irregularities, respectively.

The simplified Kalker's linear creep theory is adopted to simulate the lateral wheel-rail relationship, and the lateral wheel-rail creep force can be calculated as

$$F_{\text{y}} = -\frac{S_{22}r^{2/3}}{V}N^{2/3}\left(\dot{y}_{\text{w}} - \dot{y}_{\text{r}}\right), \tag{6}$$

where parameter $S_{22}r^{2/3}$ can be found in [27]; N is the wheel-rail normal connect force, which can be approximated as the static axle load G; $\dot{y}_{\text{w}}$ and $\dot{y}_{\text{r}}$ represent the velocity of the wheel-set and rail; V is the running speed of the train.

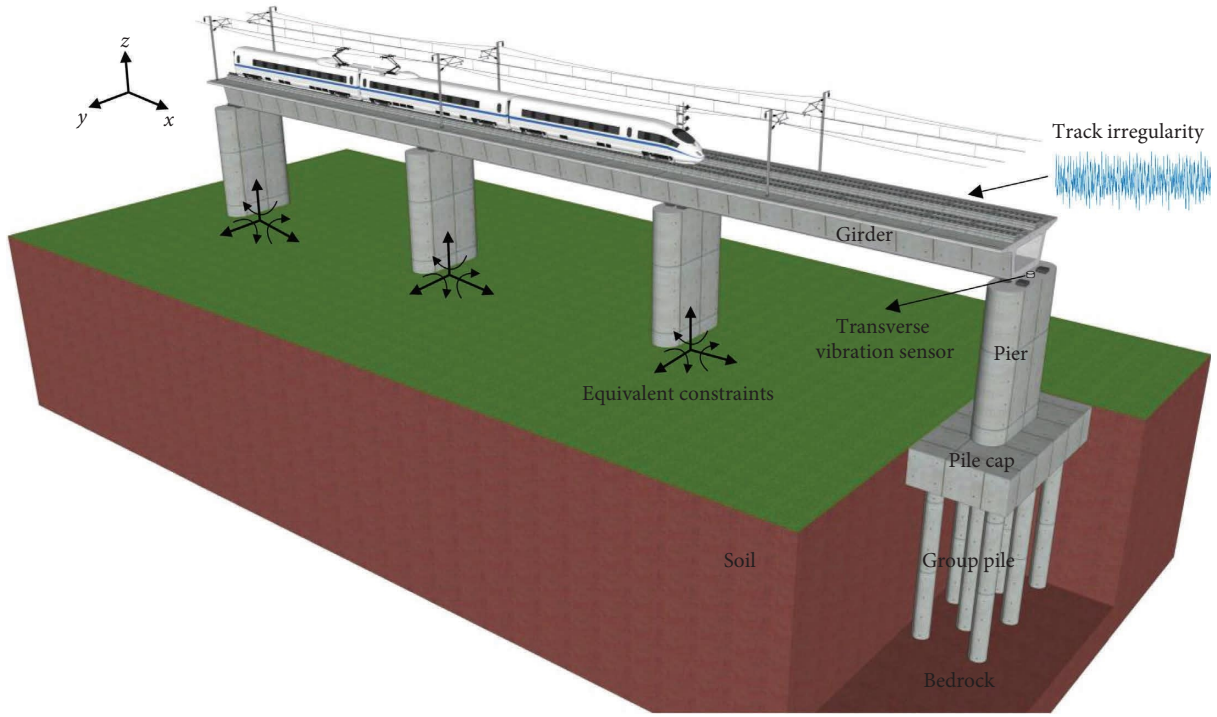

Figure 1: Schematic view of 3D HSR train-bridge-foundation system.

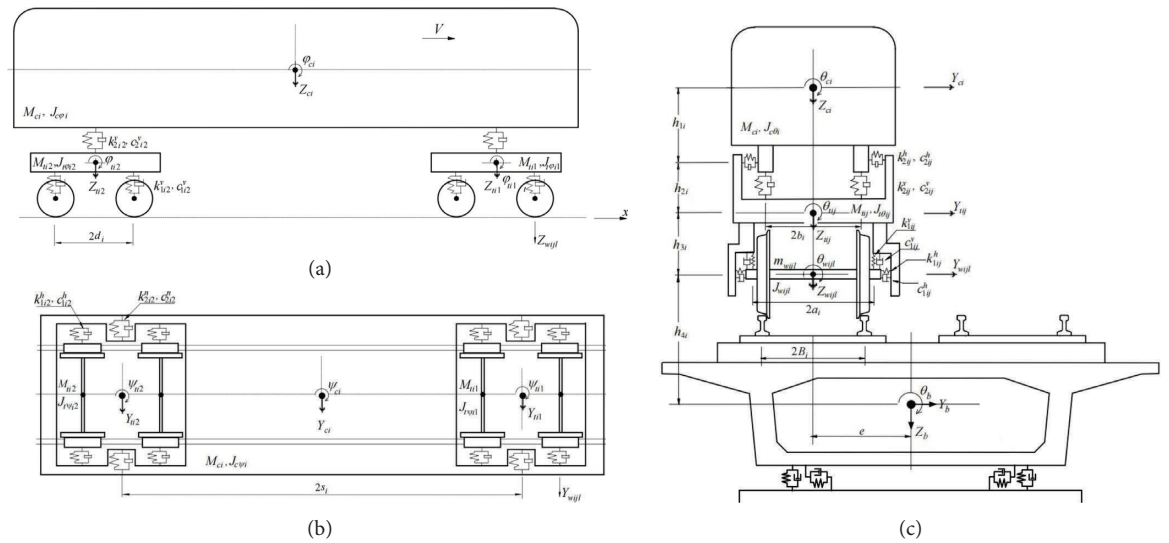

Figure 2: Schematic view of HSR train: (a) side view; (b) overhead view; (c) front view.

The track irregularities are randomly generated by Power Spectral Density functions (PSDs) of German track irregularity spectra, which have the following expressions.

Track alignment irregularity

$$S_a(\Omega) = \frac{A_a \Omega_c^2}{\left(\Omega^2 + \Omega_r^2\right)\left(\Omega^2 + \Omega_c^2\right)}. \tag{7}$$

Track vertical profile irregularity

$$S_v(\Omega) = \frac{A_v \Omega_c^2}{\left(\Omega^2 + \Omega_r^2\right)\left(\Omega^2 + \Omega_c^2\right)}. \tag{8}$$

Track cross-level irregularity

$$S_c(\Omega) = \frac{A_v b^{-2} \Omega_c^2 \Omega^2}{\left(\Omega^2 + \Omega_r^2\right)\left(\Omega^2 + \Omega_c^2\right)\left(\Omega^2 + \Omega_s^2\right)}, \tag{9}$$

where Ω is the spatial frequency; Ω_c, Ω_r, Ω_s are the cut-off frequencies; A_a and A_v are the roughness coefficients. For low disturbance irregularity, their values are $\Omega_c = 0.8246$ rad/m, $\Omega_r = 0.0206$ rad/m, $\Omega_s = 0.4380$ rad/m, $A_a = 2.119 \times 10^{-7}$ m^2·rad/m, $A_v = 4.032 \times 10^{-7}$ m^2·rad/m, $b = 0.75$ m.

On this basis, the samples of track irregularity are generated by the trigonometric series approach [27, 28], and the In-Time-Step Iteration Method is leveraged to solve the vehicle-bridge interaction problem [27, 29].

3. Quantitative Evaluation Using RD Technique and LMF Algorithm

3.1. Flexible-Base Timoshenko Beam Model for Bridge Substructure. In this section, an analytical model for interpreting the transverse dynamics of bridge substructures is theoretically derived. The vibrations in longitudinal direction are not considered in this model since the assessment of bridge pier condition mainly focuses on the transverse direction in most studies. The bridge substructure is modeled as a flexible-base Timoshenko beam with lumped mass as shown in Figure 3. Herein, two assumptions are adopted in the analytical model: (1) the transverse first-order vibration of the pier-beam system is an overall lateral oscillation, and the lumped mass allocated on the pier top takes the mass of one girder (including Phase II dead load); (2) the superstructure vibrates synchronously with the pier due to strong pier-beam coupling effect in railway bridge. The rationality of the hypothesis will be verified in subsequent numerical simulation and field tests.

The superstructure is regarded as a lumped mass on the pier top with mass of M (mass of one girder including Phase II dead load) and mass moment of inertia of J and d is the distance between the girder centroid and the pier top. The pier, characterized by a Timoshenko beam, has a height of H, a density of ρ, a cross-sectional area of A, a moment of inertia of I, an elastic modulus of E, a shear modulus of G and a shear correction factor of K. The soil-foundation interaction is represented by transverse and rotational springs with K_t and K_r, respectively. $y(x, t)$ and $\psi(x, t)$ are the transverse and rotational displacements of the pier at point x and time t.

The equations that govern the free vibration of the bridge substructure are [30, 31].

$$\begin{aligned} EI\frac{\partial^2\psi(x,t)}{\partial x^2} + KAG\left(\frac{\partial y(x,t)}{\partial x} - \psi(x,t)\right) - \rho I\frac{\partial^2\psi(x,t)}{\partial t^2} &= 0, \\ \rho A\frac{\partial^2 y(x,t)}{\partial t^2} - KAG\left(\frac{\partial^2 y(x,t)}{\partial x^2} - \frac{\partial\psi(x,t)}{\partial x}\right) &= 0. \end{aligned} \tag{10}$$

The boundary conditions can be determined as

$$\begin{aligned} &\text{at } x = 0, EI\frac{\partial\psi(0,t)}{\partial x} - K_r\psi(0,t) = 0, KAG\left(\psi(0,t) - \frac{\partial y(0,t)}{\partial x}\right) + K_t y(0,t) = 0, \\ &\text{at } x = H, EI\left(\frac{\partial\psi(H,t)}{\partial x}\right) + \left(J + Md^2\right)\left(\frac{\partial^2\psi(H,t)}{\partial t^2}\right) + Md^2\left(\frac{\partial^2 y(H,t)}{\partial t^2}\right) = 0, \\ &\text{at } x = H, KAG\left(\psi(H,t) - \frac{\partial y(H,t)}{\partial x}\right) - Md\frac{\partial^2\psi(H,t)}{\partial t^2} - M\frac{\partial^2 y(H,t)}{\partial t^2} = 0. \end{aligned} \tag{11}$$

Submitting the general solution form into the above boundary conditions yields the frequency eigenvalue equation as follows:

$$\begin{vmatrix} b\delta_1 K_r H/EI & ab\delta_1 & -a\delta_2 K_r H/EI & ab\delta_1 \\ -b\lambda^4 & abK_t H^3/EI & a\lambda^4 & abK_t H^3/EI \\ e_{31} & e_{32} & e_{33} & e_{34} \\ e_{41} & e_{42} & e_{43} & e_{44} \end{vmatrix} = 0, \tag{12}$$

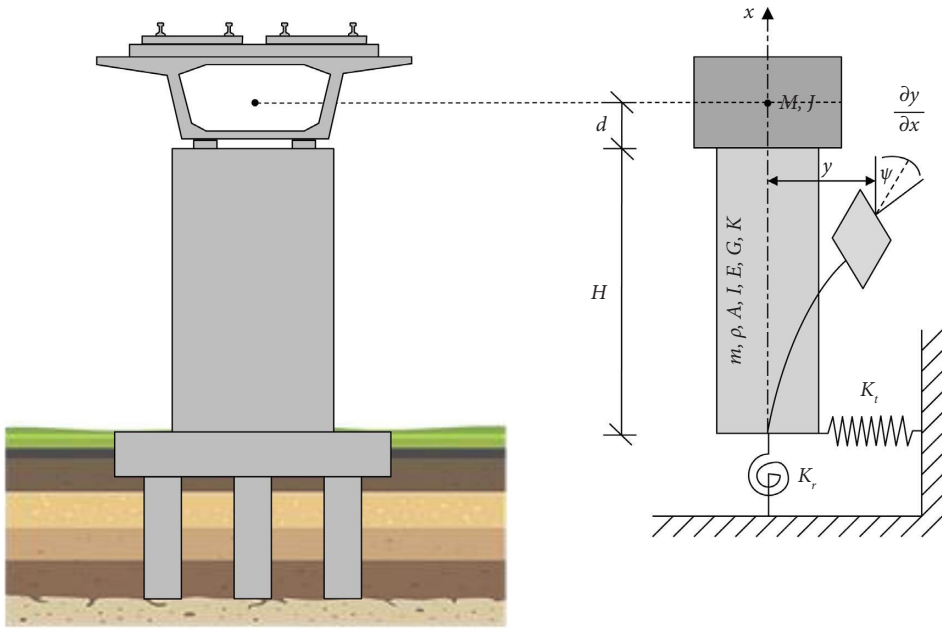

Figure 3: Flexible-base Timoshenko beam model for bridge substructure.

where $e_{31} = b[a(\delta_1 - \lambda^4\overline{md})s_1 + \lambda^4\delta_1(\overline{J} + \overline{md}^2)c_1]$, $e_{32} = b[a(\delta_1 - \lambda^4\overline{md})c_1 - \lambda^4\delta_1(\overline{J} + \overline{md}^2)s_1]$.

$e_{33} = a[b(\delta_2 - \lambda^4\overline{md})s_2 - \lambda^4\delta_2(\overline{J} + \overline{md}^2)c_2]$, $e_{34} = a[b(\delta_2 - \lambda^4\overline{md})c_2 - \lambda^4\delta_2(\overline{J} + \overline{md}^2)s_2]$.

$e_{41} = b[-\lambda^4(1 + \delta_1\overline{md})c_1 + a\lambda^4\overline{m}s_1]$, $e_{42} = b[\lambda^4(1 + \delta_1\overline{md})s_1 + a\lambda^4\overline{m}c_1]$.

$e_{43} = a[\lambda^4(1 + \delta_2\overline{md})c_2 + b\lambda^4\overline{m}s_2]$, $e_{44} = a[\lambda^4(1 + \delta_2\overline{md})s_2 + b\lambda^4\overline{m}c_2]$.

$a = \lambda^2\sqrt{(r^2 + s^2)/2 + \sqrt{(r^2 + s^2)^2/4 + (1/\lambda^4 - r^2s^2)}}$, $b = \lambda^2\sqrt{-(r^2 + s^2)/2 + \sqrt{(r^2 + s^2)^2/4 + (1/\lambda^4 - r^2s^2)}}$.

$\delta_1 = \lambda^4 s^2 - a^2$, $\delta_2 = \lambda^4 s^2 + b^2$, $s^2 = Er^2/KG$, $r^2 = I/AH^2$, $\lambda^4 = mH^3\omega^2/EI$, $\overline{m} = M/m$.

$\overline{d} = d/H$, $\overline{J} = J/mH^2$, $s_1 = \sin(a)$, $s_2 = \sinh(b)$, $c_1 = \cos(a)$, $c_2 = \cosh(b)$.

By solving equation (12) using the False Position Iteration Method [32–34] developed in MATLAB [35], the theoretical transverse natural frequencies of the bridge substructure can be obtained.

3.2. Modal Identification Using Random Decrement Technique. The RD technique is a data processing method that extracts the free vibration response of a structure from its random response, which is based on the idea of sample averaging in statistics, and utilizes the characteristics that the structural response caused by stationary random excitation has a statistical mean of zero.

Specifically, the RD function $\delta_x(\tau)$ for a single signal $x(t)$ can be obtained as according to the derivation of Cole [36].

$$\widehat{\delta}_x(\tau) = \frac{1}{N}\sum_{n=1}^{N} x(t_n + \tau) \mid C_x, \tag{13}$$

where N is the number of triggering points; $\tau = t - t_n$ is the time past the triggering time t_n; C_x: $x(t_n) = x_0$ is the triggering condition and x_0 is the trigger level as shown in Figure 4.

Vandiver et al. [37] laid a theoretical basis of the RD function and equation (13) can be rewritten in a conditional expectation form as

$$\delta_x(\tau) = E[x(t_n + \tau) \mid x(t_n) = x_0], \tag{14}$$

where the triggering condition is usually taken by the users in the range of $(1\sim2)\sigma_x$, and σ_x is the standard deviation of the signal $x(t)$.

Then, the free vibration response can be processed by the Fast Fourier Transform (FFT) to yield the frequency response as

$$F(\omega) = \mathrm{FFT}\{\hat{\delta}_x(\tau)\}, \tag{15}$$

where ω denote the frequency.

3.3. Levenberg–Marquardt–Fletcher Algorithm. Using the RD method, the free vibration and modal parameters of the bridge substructure can be extracted. It is assumed that the pier body is intact and the transverse and rotational stiffness decrease in the same proportion [24], the unknown condition indicator is defined as $\beta = K_e/K_d$ to describe the weakening degree of the bridge foundation caused by scour and freeze-thaw cycle, where K_e and K_d denote the tested and designed stiffness at pier bottom, respectively. To quantify the health condition of the substructures, herein, the LMF algorithm [38] is leveraged to achieve rapid system identification, which is more stable and efficient for solving nonlinear least squares problems. This system identification problem can be considered as an optimization problem

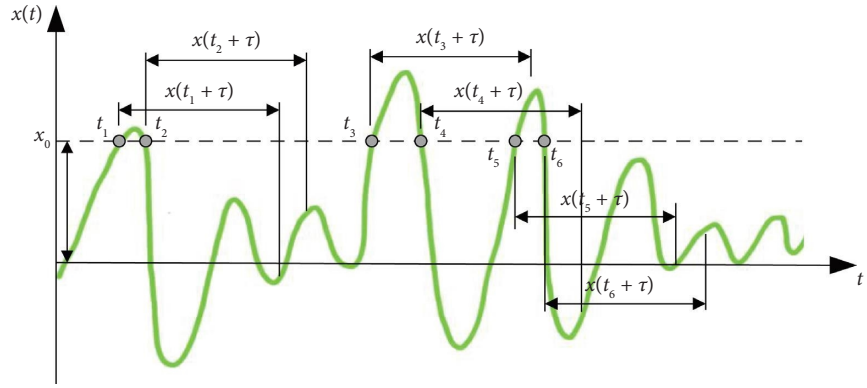

Figure 4: Schematic view of the RD method.

which seeks to find the optimum solution β^* that minimizes the following objective function:

$$F(\beta) = \left\| \frac{f_1^2(\beta) - \tilde{f}_1^2}{\tilde{f}_1^2} \right\|_2^2 = \|r\|_2^2 = r^{\mathrm{T}} r, \tag{16}$$

where $\tilde{f}_1$ is the tested first-order transverse frequency of the substructure; f_1 is the theoretical first-order transverse frequency calculated by the flexible-base Timoshenko beam model; r is the residual function.

β^* that minimizes the objective function should satisfy the following necessary conditions

$$\frac{\partial \|r\|_2^2}{\partial \beta} = 2\frac{\partial r^{\mathrm{T}}}{\partial \beta} r = 2\mathbf{J}^{\mathrm{T}} r = 0, \tag{17}$$

where $\mathbf{J} = \partial r / \partial \beta$ is called Jacobian matrix.

The update equation of the optimized parameter β at step $(k+1)$ can be described as

$$\begin{aligned} \beta^{(k+1)} &= \beta^{(k)} + \Delta\beta^{(k)}, \\ \Delta\beta^{(k)} &= -\left(\mathbf{J}^{(k)T}\mathbf{J}^{(k)} + \lambda^{(k)}\mathbf{D}\right)^{-1}\mathbf{J}^{(k)} r^{(k)}, \end{aligned} \tag{18}$$

where $\lambda^{(k)}$ is a scale parameter; $\mathbf{D}$ is a suitable diagonal matrix of scales, which is usually chosen as an identity matrix $\mathbf{I}$ or a diagonal of the matrix $\mathbf{A} = \mathbf{J}^{\mathrm{T}}\mathbf{J}$.

Let the residuals $r(\beta)$ are smooth functions, then its Taylor series expansion can be deduced as equation (19), and the Jacobian matrix $\mathbf{J}$ can be calculated as equation (20):

$$r^{(k+1)} = r^{(k)} + \frac{\partial r^{(k)}}{\partial \beta^{(k)}} \Delta\beta^{(k)} + \cdots, \tag{19}$$

$$\mathbf{J}^{(k)} = \frac{\partial r^{(k)}}{\partial \beta^{(k)}} \approx \frac{r^{(k+1)} - r^{(k)}}{\Delta\beta^{(k)}}. \tag{20}$$

The entire optimization iteration process starts with a suitable guess $\beta^{(0)}$, and the iteration procedure is continued until

$$|\beta^{(k+1)} - \beta^{(k)}| < \varepsilon, \quad k < N, \tag{21}$$

where ε is the admissible tolerance; N is the maximum number of iteration step.

3.4. Procedure of the Methodology. Figure 5 illustrates the overall procedure of the proposed methodology, which is composed of the RD technique and LMF algorithm with a newly developed flexible-base Timoshenko beam model for bridge substructure. The RD method is leveraged to extract the free vibration of the bridge substructure, and the modal parameters can be further obtained by using the FFT. The theoretical solution of modal parameters can be derived from the flexible-base Timoshenko beam model, and the spring stiffnesses at pier bottom are constructed as an indicator to reflect the foundation state. The LMF continuously estimates the optimal parameters until the algorithm convergence is completed. The proposed methodology is a model-based output-only approach using only one vibration transducer installed on the pier top and does not require any information about the unknown excitation.

4. Numerical Validation

4.1. Numerical Model Specification. A three-span double-track simply supported HSR bridge with a standard span of 32 m is established in this part. Prestressed concrete box girders and round-ended reinforced concrete piers are adopted with the cross-sectional dimension as shown in Figure 6. The strength grade of the concrete for the girder and pier are C50 and C35 in Chinese code, respectively (the corresponding elastic modulus are 3.45×10^4 MPa and 3.15×10^4 MPa). The density of the concrete is 2500 kg/m^3, and Poisson's ratio is 0.2. The China's CRTS-I ballastless track system is used to consider the Phase II dead load. According to the design information, the total mass of one girder (Phase I + Phase II dead load) is calculated as 1290.74 t. The KTPZ-1-6000 type pot rubber bearings are adopted in the bridge model, whose friction coefficient is 0.05 and vertical stiffness is 1.376×10^{12} N/m [39]. Underneath each pier are 6 restraint springs representing 6 DOFs equivalent stiffnesses provided by the group pile foundation, which can be determined by the geological information and are presented in Table 1. The bridge model

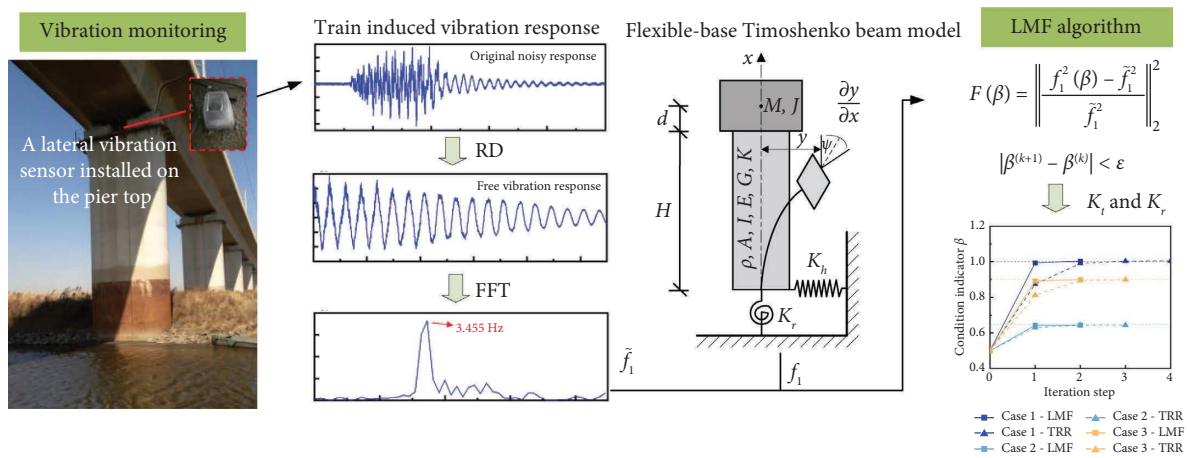

Figure 5: Procedure of the proposed methodology.

is established in ANSYS 2021R1 software, and Beam 188 element, considering the effect of shear deformation is adopted to construct the beams and piers. The beams and piers are modeled using parameterization and divided into 32 and 10 elements, respectively. Linear spring damping element Combine14 is adopted to simulate the bearings and foundation bottom constraints. The bridge damping ratio of 0.02 is adopted in the model. The boundary conditions of the outer beams are set as simply supported.

The marshaling train is consisted of four locomotives (L) and four trailers (T) with the layout form (L + T + L + T + T + L + T + L), and the parameters of the train model are listed in Table 2. The generated track irregularity samples are shown in Figure 7. The marshaling trains pass the bridge at a constant speed of 300 km/h and travel for 100 m before entering the bridge to stabilize the vibration of the vehicle body. The sampling frequency is 1000 Hz, and the total time history is set to 10 s. The transverse acceleration responses on the top of Pier 1 and Pier 2 are measured to conduct the validation of the proposed quantitative evaluation method.

4.2. Verification of the Proposed Analytical Model and Modal Identification Method. To validate the effectiveness of the proposed method, three scenarios considering single condition degradation, multiple condition degradation, and varying pier heights have been set, as detailed in Table 3. Using Case 3 as an illustration, the modal analysis of the bridge-foundation system is conducted using the block Lanczos method [40]. The first two transverse mode shapes and frequencies of the bridge-foundation system for Case 3 are shown in Figure 8. It can be observed that the first two vibrations of the pier-beam system are in order manifested as an overall lateral oscillation and a lateral reverse vibration of adjacent piers, and the same pattern can be found for both Case 1 and Case 2, which preliminarily validates the model assumptions in Section 3.1.

The measured acceleration responses on the pier top are contaminated by Gaussian white noise with 5% variance in root mean square (RMS) to consider the influence of environmental noise

$$x_n = x_c + E_p N_0 \sigma(x_c), \tag{22}$$

where x_n is the noisy acceleration signal, E_p is the noise level, N_0 is the standard normal distribution vector with a mean value of zero and a unit standard deviation, x_c is the clean acceleration signal, and $\sigma(x_c)$ is its standard deviation.

A trigger point of $1.2\sigma(x(t))$ and a number of triggering points of 5500 are selected for the RD implementation with a corresponding segment length equal to 5.5 s. The original noisy responses on the pier top, the extracted free vibration responses, and the corresponding modal analysis results of different cases are shown in Figure 9. It can be seen that the first order transverse frequency of the bridge substructure can be successfully identified from the extracted free vibration response by picking up the frequency at the first peak. However, the higher order frequencies are still difficult to distinguish due to interference from multiple frequency peaks, which is related to the complexity of train lateral excitation and the spatial coupling vibration of multispan bridges. Table 4 presents the modes calculated by the Euler–Bernoulli beam model used in [3] and the proposed model in this paper. By comparing the results with the reference value extracted by random decrement—Fast Fourier Transform (RD-FFT), it can be concluded that the Timoshenko beam model has higher computational accuracy than the Euler–Bernoulli beam model, particularly for low piers. Fairly good agreement is obtained between the results of reference value identified from the local pier beam system and those calculated by the Timoshenko beam analytical model. Therefore, the proposed flexible-base Timoshenko beam model is highly suitable for the modal analysis and quantitative evaluation of bridge substructures.

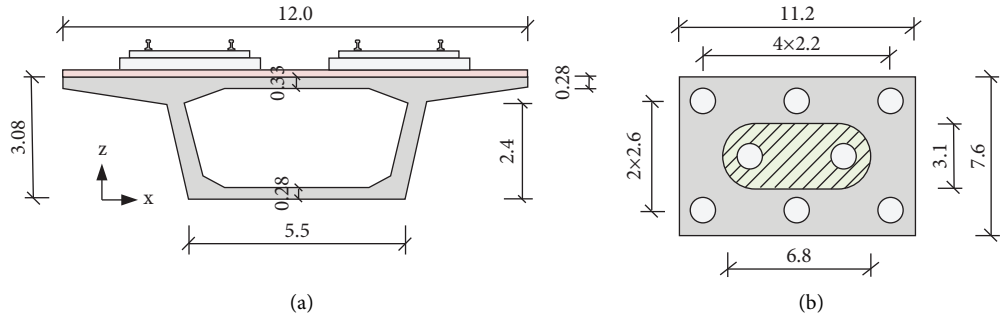

Figure 6: Cross-sectional dimension: (a) girder; (b) pier and piles. (Unit: m).

Table 1: Equivalent spring stiffness at pier bottom.

Type	Translational springs (N/m)			Torsional springs (N/(m·rad))		
	K_x	K_y	K_z	K_{rx}	K_{ry}	K_z
Value	9.707×10^8	9.328×10^8	8.317×10^9	8.316×10^{10}	4.657×10^{10}	1.455×10^{10}

Table 2: Parameters for the train model.

Parameters of the ith vehicle	Unit	Locomotive	Trailer
Car body mass (M_c)	kg	4.8×10^4	4.4×10^4
Pitch mass moment of car body ($J_{c\varphi}$)	kg·m^2	2.7×10^6	2.7×10^6
Roll mass moment of car body ($J_{c\theta}$)	kg·m^2	1.15×10^5	1.0×10^5
Yaw mass moment of car body ($J_{c\psi}$)	kg·m^2	2.7×10^6	2.7×10^6
Bogie mass (M_t)	kg	3.2×10^3	2.4×10^3
Pitch mass moment of bogie ($J_{t\varphi}$)	kg·m^2	7.2×10^3	2.2×10^3
Roll mass moment of bogie ($J_{t\theta}$)	kg·m^2	3.2×10^3	1.8×10^3
Yaw mass moment of bogie ($J_{t\psi}$)	kg·m^2	6.8×10^3	2.2×10^3
Wheel-set mass (M_w)	kg	2.4×10^3	2.4×10^3
Roll mass moment of bogie ($J_{w\theta}$)	kg·m^2	1.2×10^3	1.1×10^3
Yaw mass moment of bogie ($J_{w\psi}$)	kg·m^2	1.2×10^3	1.1×10^3
Lateral stiffness of primary suspension (k_1^{h})	N/m	3.0×10^6	5.0×10^6
Vertical stiffness of primary suspension (k_1^{v})	N/m	1.04×10^6	7.0×10^5
Lateral damping of primary suspension (c_1^{h})	N·s/m	0	0
Vertical damping of primary suspension (c_1^{v})	N·s/m	5.0×10^3	5.0×10^3
Lateral stiffness of secondary suspension (k_2^{h})	N/m	2.4×10^5	2.8×10^5
Vertical stiffness of secondary suspension (k_2^{v})	N/m	4.0×10^5	3.0×10^5
Lateral damping of secondary suspension (c_2^{h})	N·s/m	3.0×10^4	2.5×10^4
Vertical damping of secondary suspension (c_2^{v})	N·s/m	6.0×10^3	6.0×10^3
Full length of train (L_c)	m	24.775	24.775
Lateral span of primary suspension ($2a_i$)	m	2.0	2.0
Lateral span of secondary suspension ($2b_i$)	m	1.9	1.9
Distance of two wheel-sets ($2d_i$)	m	2.5	2.5
Distance of two bogies ($2s_i$)	m	17.375	17.375
Distance from car-body to secondary suspension (h_1)	m	0.8	0.8
Distance from secondary suspension to bogie (h_2)	m	0.3	0.3
Distance from bogie to wheel-set (h_3)	m	0.14	0.14

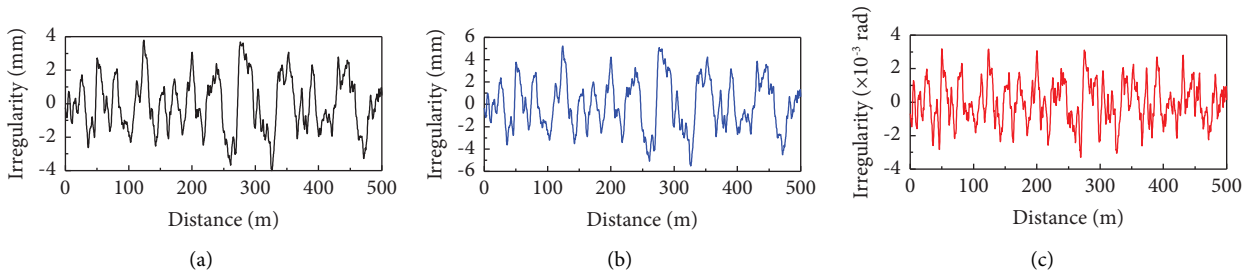

Figure 7: Generated track irregularity samples: (a) alignment irregularity; (b) vertical profile irregularity; (c) cross-level irregularity.

Table 3: Case settings and description.

Case no.	Pier height (m)	Scenario settings	Description
1	5	$\beta = 1$ at Pier 1 and $\beta = 1$ at Pier 2	Intact
2	5	$\beta = 0.65$ at Pier 1 and $\beta = 1$ at Pier 2	Single condition degradation
3	8	$\beta = 0.9$ at Pier 1 and $\beta = 0.9$ at Pier 2	Multiple condition degradation

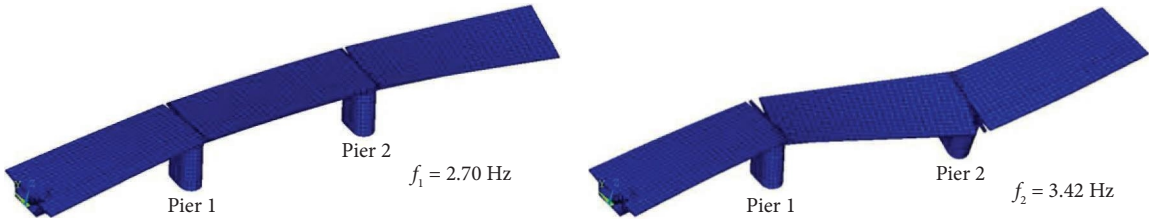

Figure 8: The first two transverse mode shapes and frequencies of the bridge-foundation system for case 3.

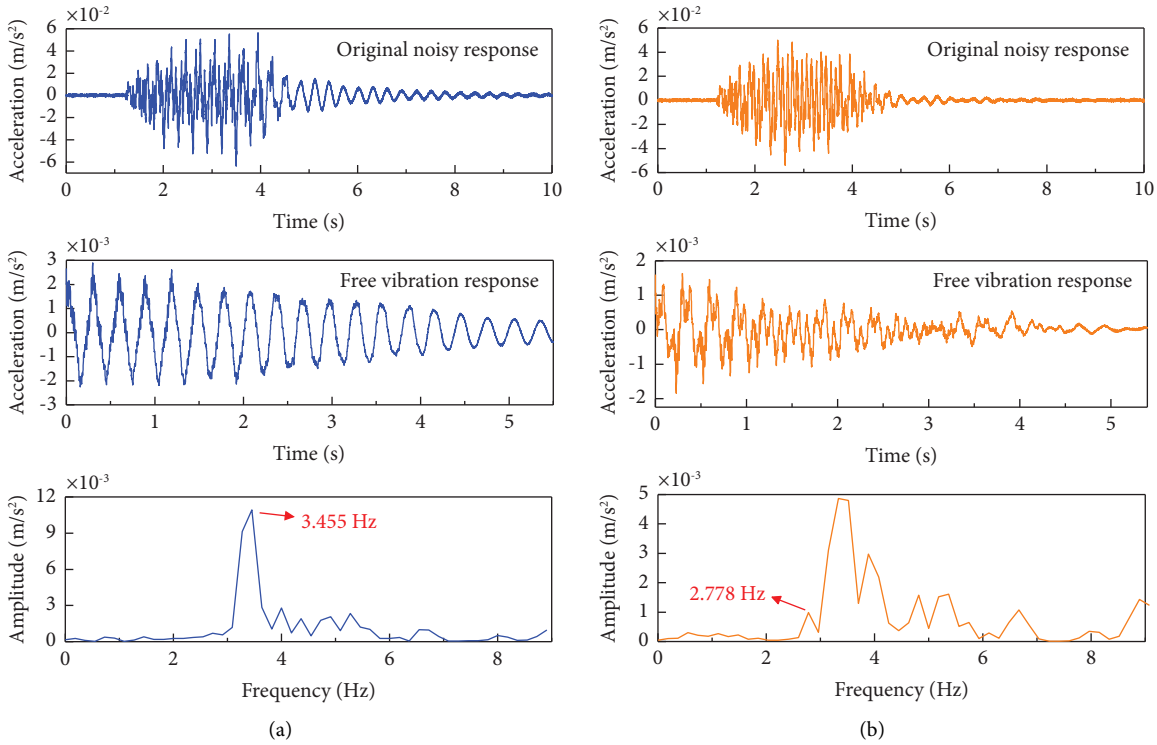

Figure 9: Continued.

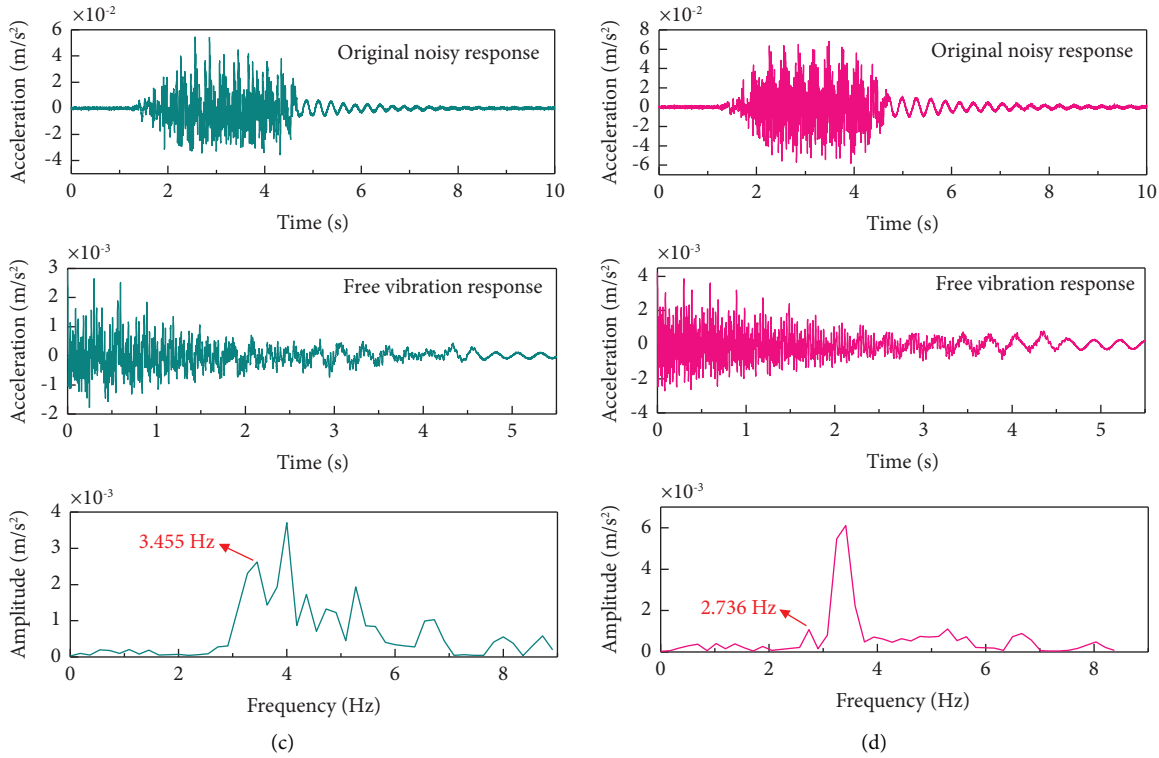

Figure 9: The analysis results of different cases: (a) pier 1 in case 1; (b) pier 1 in case 2; (c) pier 2 in case 2; (d) pier 2 in case 3.

Table 4: Comparison of results for the first two modes using different models.

	Mode	Pier 1		Pier 2	
		1st order	2nd order	1st order	2nd order
Case 1	Reference (RD-FFT)	3.455	—	3.455	—
	Timoshenko beam model	3.448	28.673	3.448	28.673
	Euler–Bernoulli beam model	3.470	29.051	3.470	29.051
Case 2	Reference (RD-FFT)	2.778	—	3.455	—
	Timoshenko beam model	2.792	23.484	3.448	28.673
	Euler–Bernoulli beam model	2.803	23.691	3.470	29.051
Case 3	Reference (RD-FFT)	2.736	—	2.736	—
	Timoshenko beam model	2.735	17.116	2.735	17.116
	Euler–Bernoulli beam model	2.734	17.330	2.734	17.330

4.3. Verification of the Proposed Condition Evaluation Method. In the implementation of LMF, the initial value of $\beta^{(0)}$ is 0.5, and its lower and upper bounds are set to 0 and 2 to ensure that the identified parameters have physical meaning. The termination tolerance $\varepsilon = 10^{-9}$, and the maximum number of iterations allowed $N = 20$. Furthermore, the trust region reflective (TRR) Gaussian Newton algorithm adopted in [24] is also conducted to make a comparison with the LMF algorithm utilized in this study. It can be seen from Figure 10(a) and Table 5 that both LMF and TRR can achieve satisfactory identification accuracy with an error of less than ±1%. Of note, the LMF algorithm has higher identification accuracy and smaller error than TRR, indicating that it is superior in condition quantification. In addition, Figure 10(b) shows the condition iteration process for pier 1. It can be seen that the LMF algorithm converges in just two steps under all setting scenarios, while TRR requires three or more steps, which demonstrates that the LMF needs less computation time. Good computational performance and efficiency facilitate online system identification and quantitative assessment of railway bridge substructures.

5. Real-World Application

5.1. Bridge Overview. To investigate the performance of the proposed method in actual bridges, the 2nd Songhua River bridge located on the Harbin–Dalian HSR is served as a real-world case study. The Harbin–Dalian HSR traverses the coldest regions in China, experiencing a minimum air temperature of −39.9°C and a maximum soil freezing depth of 2.05 m. Compared to nonfreeze-thaw regions, the unique

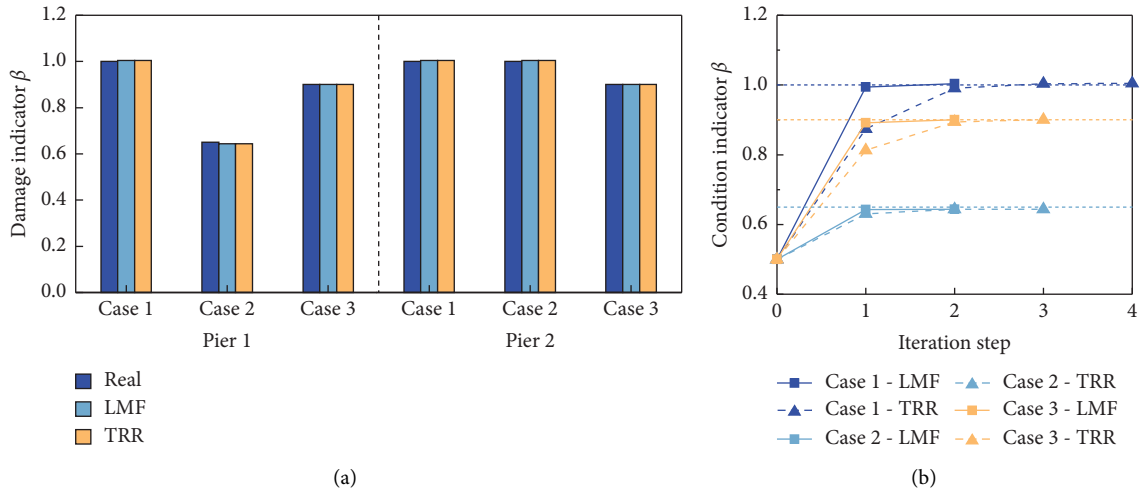

Figure 10: The identified results using different algorithms: (a) identified results for pier 1 and pier 2; (b) condition iteration process for pier 1.

Table 5: Comparison of the identified results using different algorithms.

Results		Pier 1			Pier 2		
		Real	Identified	Error (%)	Real	Identified	Error (%)
Case 1	LMF	1.0000	1.0040	0.40	1.0000	1.0040	0.40
	TRR	1.0000	1.0045	0.45	1.0000	1.0045	0.45
Case 2	LMF	0.6500	0.6436	−0.98	1.0000	1.0040	0.40
	TRR	0.6500	0.6438	−0.95	1.0000	1.0045	0.45
Case 3	LMF	0.9000	0.9002	0.02	0.9000	0.9002	0.02
	TRR	0.9000	0.9007	0.08	0.9000	0.9007	0.08

frost heave and freeze-thaw effects in severe cold regions are more likely to cause problems such as bridge foundation damage and insufficient bearing capacity. The test piers 453#~457# were constructed on the side of Yinma River in Dehui City, Jilin Province, of which the piers 454#~456# are underwater as shown in Figure 11. The three bridge pile caps are exposed to air, and the soil on the river side of the bridge pier is perennially eroded by the flowing water. The moisture content of the foundation soil on both lateral sides of the bridge pier is notably different and is significantly influenced by freeze-thaw phenomena.

The superstructure and piers adopt a 32.6 m length double line simply supported box girder and round-ended piers, respectively. The strength grade of the concrete for the girder and pier are C50 and C35 in Chinese code, respectively (the corresponding elastic modulus are 3.45×10^4 MPa and 3.15×10^4 MPa). The density of the concrete is 2500 kg/m^3, and Poisson's ratio is 0.2. China's CRTS-I ballastless track system is used to consider the Phase II dead load. According to the design information, the total mass of one girder (Phase I + Phase II dead load) is calculated as 1290.74 t. The bored piles with a length of 42 m and a diameter of 1.25 m are symmetrically arranged about the center of the platform and have the same layout and sizes of group-piles as shown in Figure 6(b). The heights of piers 453#~457# are 16.5 m, 20 m, 20 m, 20 m, and 17 m, respectively, and the height of pile cap is 3 m.

5.2. Field Tests and Feasibility Verification. The impact vibration test and train-induced vibration test were conducted to verify the feasibility of the proposed modal analysis method for bridge substructures. In the tests, a INV3018C 24-bit data acquisition instrument equipped with 28 channels was utilized to collect the dynamic signals, each of which has a maximum sampling frequency of 102.4 kHz. The 941B multifunctional vibration sensor was adopted to measure the structural response on the pier top. It comprises four gears, namely acceleration, microvelocity, medium velocity, and high velocity, designed to operate normally in temperatures ranging from −35°C to 70°C. In the experiment, a microvelocity gear was utilized, featuring a sensitivity of 23 V·s/m, a maximum range of 0.125 m/s, a passband of 1~100 Hz, and a resolution ratio of 4×10^{-8} m/s. The sampling frequency was set to 512 Hz.

The impact vibration test utilized a 30 kg cast iron heavy hammer to apply excitation, and the heavy hammer was wrapped in a hard rubber ring to safeguard the bridge

Figure 11: Schematic of pier 453#~457# in the 2nd Songhua River bridge.

structure from any damage inflicted by the impact force. During the experiment, a rope can be utilized to secure the heavy hammer at the entrance ladder of the beam, and it can be struck from the middle of the pier top to one side to generate lateral vibration of the bridge pier. The layout plan for the measurement points is shown in Figure 12.

The time history of transverse velocity on the top of pier 455# (measurement point 3) under the impact of the heavy hammer is depicted in Figure 13(a). It can be seen that the heavy hammer can effectively stimulate the lateral vibration of the bridge pier, and the free decaying signal of the bridge pier is obvious. Figure 13(b) compares the lateral response of the pier top (measurement point 3) and the beam end (measurement point 12). From the observations made, it is evident that the measurement points located at the top of the pier and at the end of the beam exhibit synchronous vibration at the same phase, indicating that the pot rubber bearing has a notable lateral shear stiffness, and the vibration coupling effect between the pier and beam is strong. This also confirms the rationality of the model assumption found in Section 3.1.

The impact vibration test method (IVTM) [41] was utilized to analyze the frequency spectrum of pier 455#, and the results are depicted in Figure 14. The figure reveals that multiple peak points meet the phase angle condition, with values of 2.38 Hz, 2.88 Hz, 3.25 Hz, and 3.88 Hz, respectively. Furthermore, by combining the responses of additional measurement points, stochastic subspace identification (SSI) [42] was employed to determine the mode of the multispan simply supported beam system. Consequently, the stability diagram is obtained as Figure 15, where the stable axis, constituting a frequency of the system, is composed of various stable points of different modal orders. In the stabilization diagram, *f*, *d*, and *v*, respectively, indicate that the frequency, damping, and mode shapes are stable, and the symbol ⊕ denotes that all three vectors are stable simultaneously. Accordingly, the first four modes dominated by lateral vibration of the bridge pier are depicted in Figure 16: (1) a lateral overall swing of the entire bridge (2.38 Hz); (2) lateral local vibration of piers (2.87 Hz); (3) lateral local vibration of piers in reverse direction (3.27 Hz); (4) a lateral staggered vibration of the entire bridge (3.94 Hz). It can be concluded that the modes identified by IVTM and SSI are highly consistent, and both methods can effectively identify the modes of the substructure. By processing the measured train-induced response on the top of pier 455# using RD-FFT, the first mode can be successfully extracted as shown in Figure 17. The trigger point is set as $\sqrt{2}\sigma(x(t))$ and the number of triggering points is 6000. The extracted modal frequency 2.39 Hz matches well with those identified by IVTM and SSI, confirming the precision and viability of the suggested approach.

In addition, to further verify the applicability and accuracy of the proposed modal identification method for the railway simply supported beam bridge substructures, in-situ dynamic tests were conducted on bridge piers at various heights and locations. The identification results of each central bridge pier are presented in Table 6. The results indicate that the RD-FFT method has high accuracy and robustness in identifying the transverse fundamental

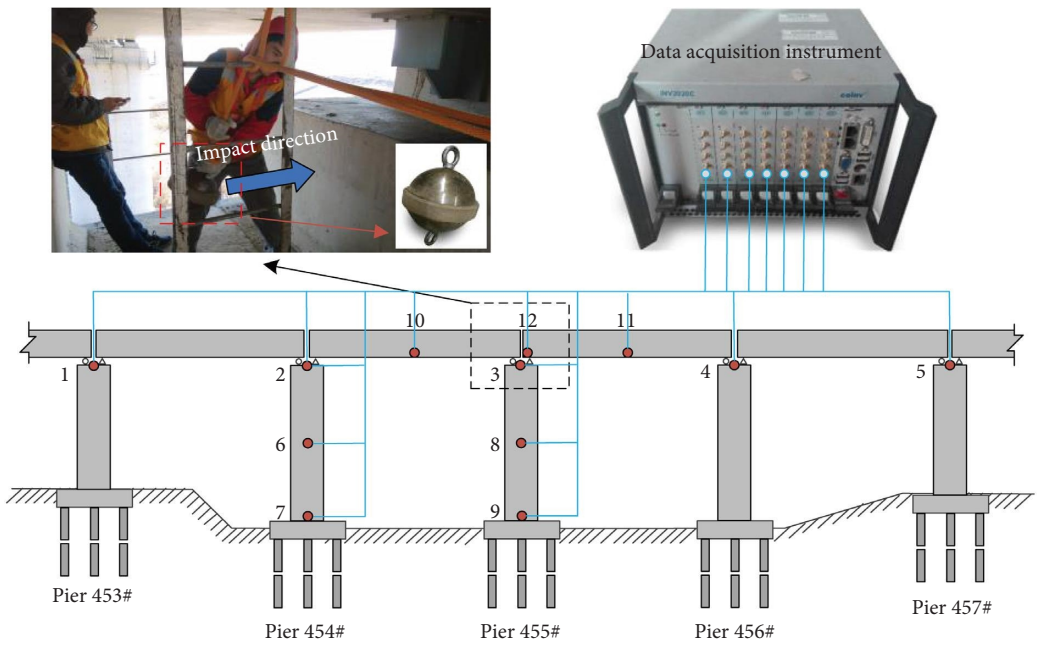

Figure 12: The excitation and data acquisition equipment and layout plan of measurement points.

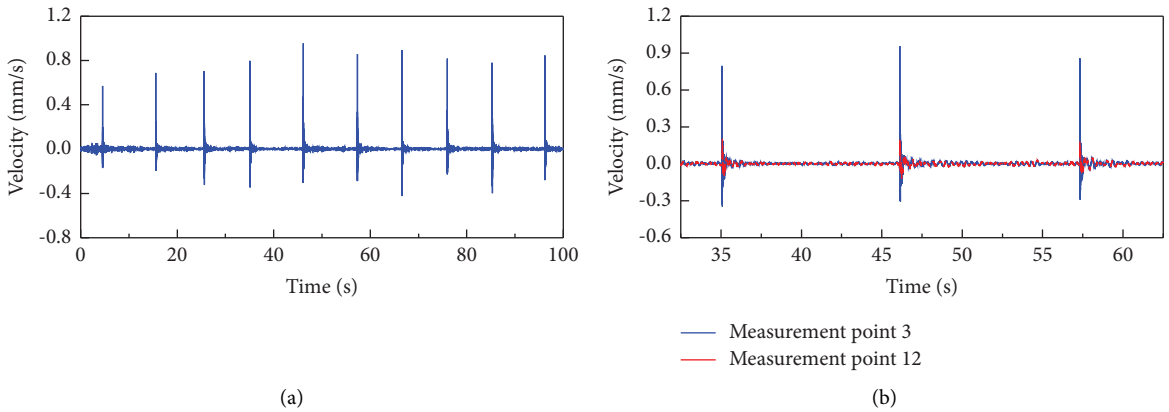

Figure 13: Transverse velocity time histories: (a) at the top of pier 455#; (b) at measurement points 3 and 12.

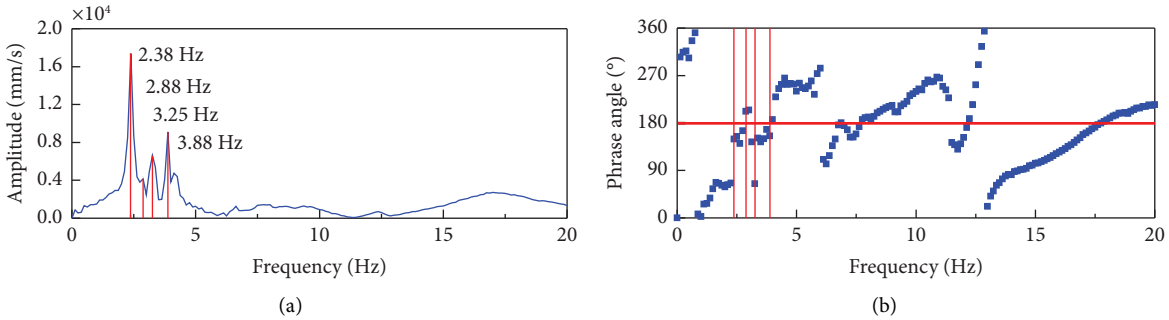

Figure 14: The modal analysis results of pier 455# top measurement point using IVTM.

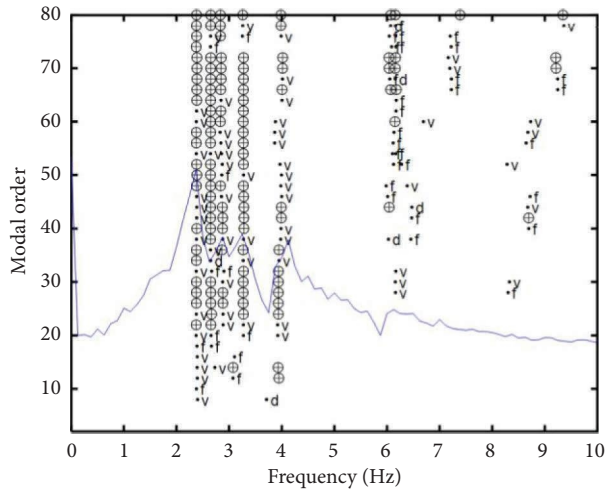

Figure 15: Stabilization diagram for modal identification using SSI.

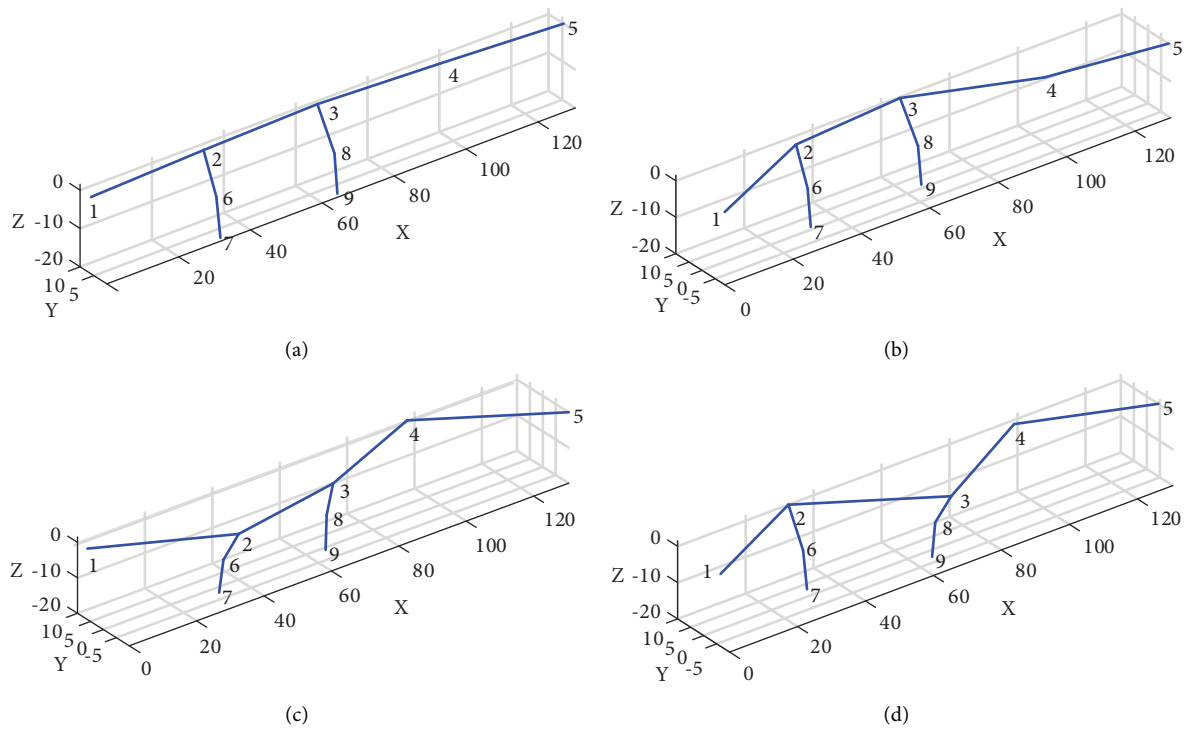

Figure 16: The identified modes using SSI: (a) the first mode shape (2.38 Hz); (b) the second mode shape (2.87 Hz); (c) the third mode shape (3.27 Hz); (d) the fourth mode shape (3.94 Hz).

frequency of the local pier-beam system and facilitates online system identification and condition evaluation on in-service bridge substructures by using only one vibration sensor.

5.3. Condition Monitoring and Quantitative Evaluation of Bridge Substructure. The dominant factors affecting the occurrence and development of seasonal freezing and thawing in severe cold regions are the environmental conditions of frozen soil. The maximum seasonal depth of freezing along the test area is 1.82 m, which commences freezing in late October and completely melts by the end of May of the following year. The periodic variation of temperature can roughly divide the region's freezing and thawing stages into nonfreezing period (from June to October), freezing development period (from November to December), freezing stationary period (from January to February), and thaw period (from March to May). Therefore, in this section, we have applied the proposed method to

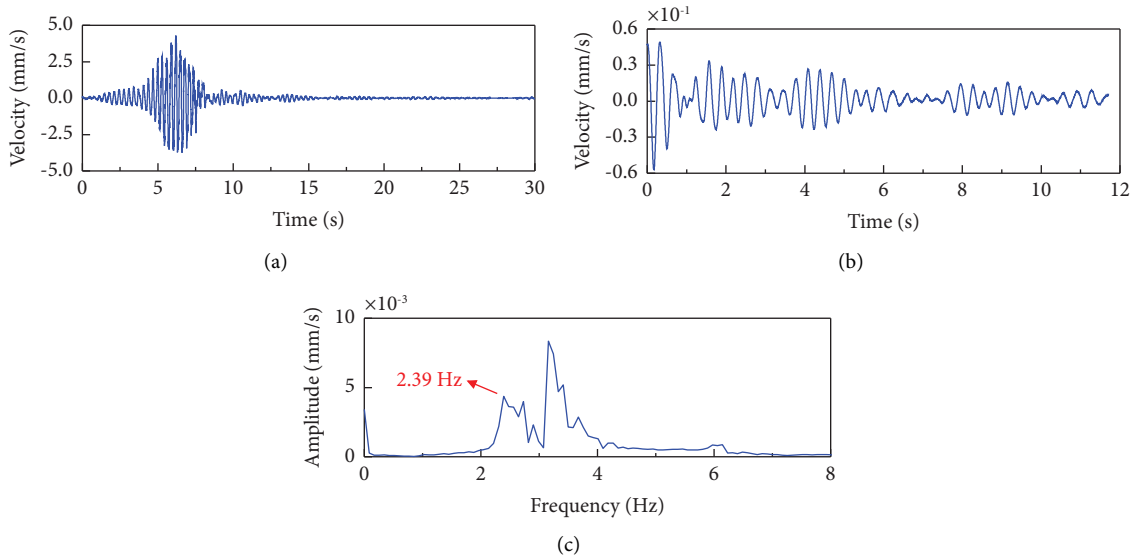

Figure 17: The modal identification results using RD-FFT: (a) the measured train-induced response on the top pf pier 455#; (b) the extracted free vibration response; (c) frequency spectrum of the free vibration response.

Table 6: Comparison of results for the first mode identified by different methods.

Pier no.	Height (m)	Pile cap height (m)	The first mode (Hz)		
			IVTM	SSI	RD-FFT
148#	6.0	2.5	3.50	3.47	3.50
248#	11.5	2.5	2.63	2.63	2.65
445#	20.5	3.0	2.13	2.14	2.13

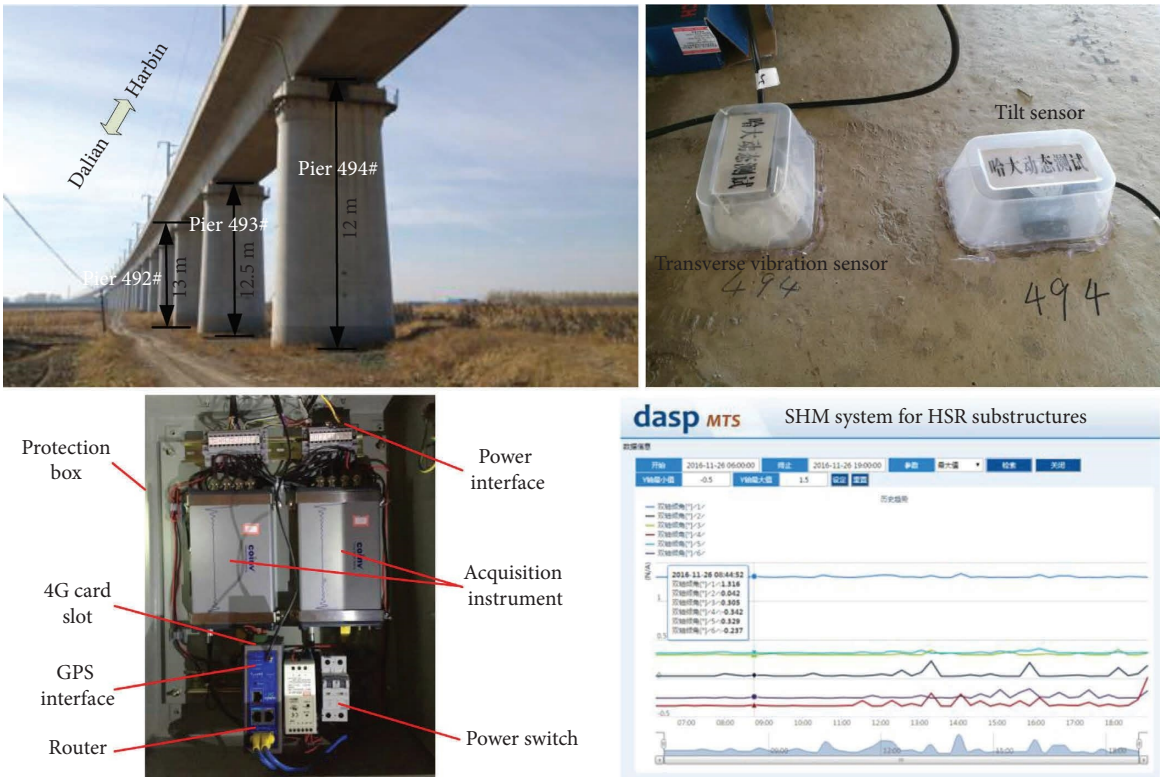

Figure 18: Schematic of pier 492#~494# in the 2nd Songhua River bridge and the SHM system.

Table 7: Results of the investigation of the in-situ geological environment.

Pier no.	Upper interface (m)	Lower interface (m)	Soil categories	m and m_0 (MPa/m^2)
494#	0	10.700	Fine sand, silty clay	10
	10.700	21.063	Medium sand, gravel	55
	21.063	Pile-bottom	Mudstone, sandstone interbedded	100

Table 8: Equivalent spring stiffness at the bottom of pier 494#.

Type	Translational springs (N/m)			Torsional springs (N/(m·rad))		
	K_x	K_y	K_z	K_{rx}	K_{ry}	K_{rz}
Value	9.517×10^8	9.372×10^8	1.283×10^{10}	1.513×10^{11}	7.663×10^{10}	1.702×10^{10}

Table 9: Normal value of lateral amplitude at the top of HSR bridge piers in Chinese code [43].

Design speed of the line (km/h)	Normal value (mm)	Scope of application
250	$H_p/55B + 0.02$	$0.5 \le H_p/B \le 4.2$
350	$H_p/60B + 0.03$	

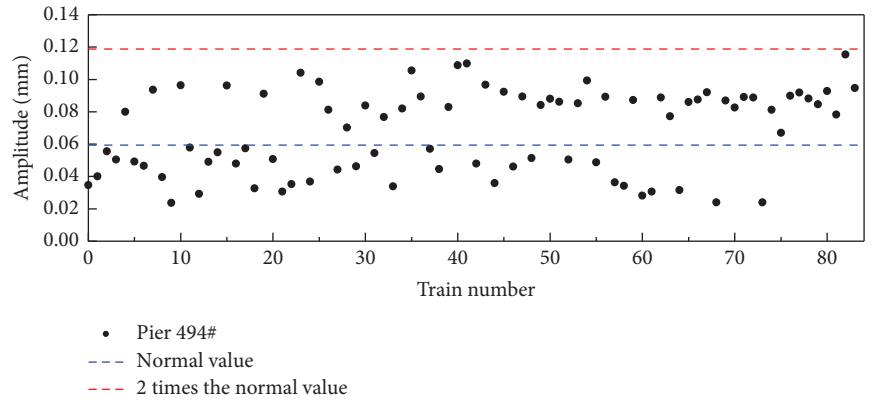

Figure 19: Daily statistical diagram of amplitude at the top of pier 494# (October 25th).

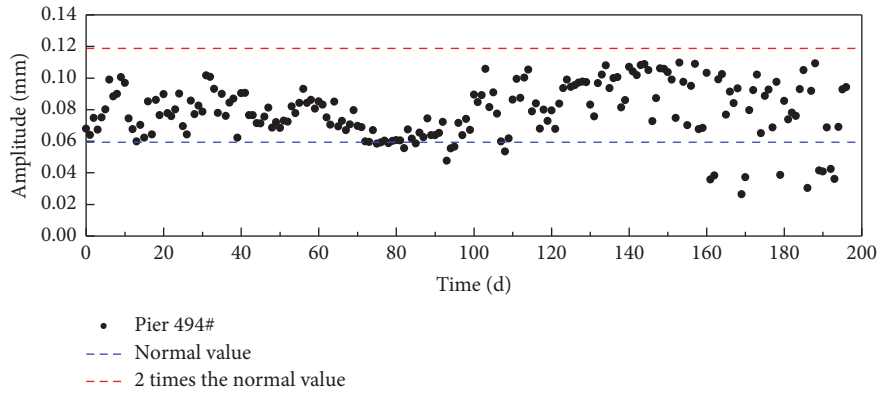

Figure 20: Evolution diagram of amplitude at the top of pier 494# during the entire monitoring period.

a built online structural health monitoring system. The train-induced responses on the top of piers 492#~494# were continuously measured for 197 days, starting from October 25th to May 9th of the following year. The adopted monitoring equipment and platform are shown in Figure 18, which is composed of two 4-channel acquisition devices, router, GPS antennas, 4G cards, signal access connectors, and protection box. The collected response data of each

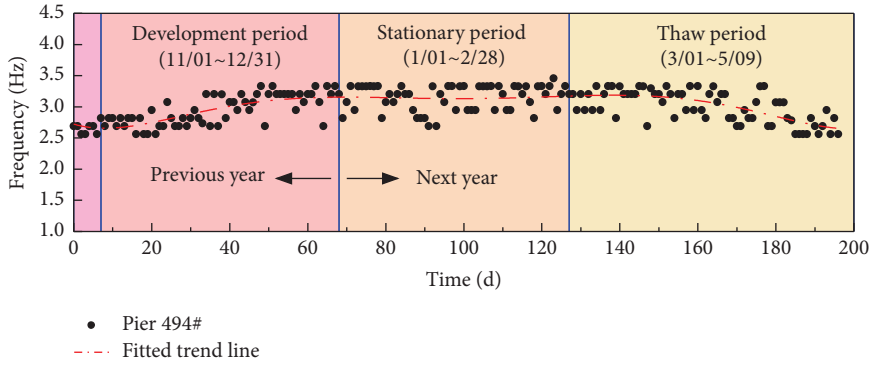

Figure 21: Evolution diagram of the lateral natural frequencies of pier 494# extracted by RD-FFT during the entire monitoring period.

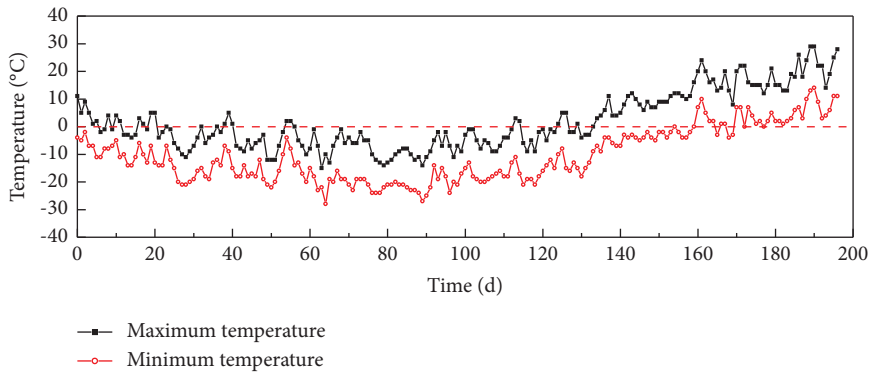

Figure 22: Temperature data at the tested bridge recorded during the entire monitoring period.

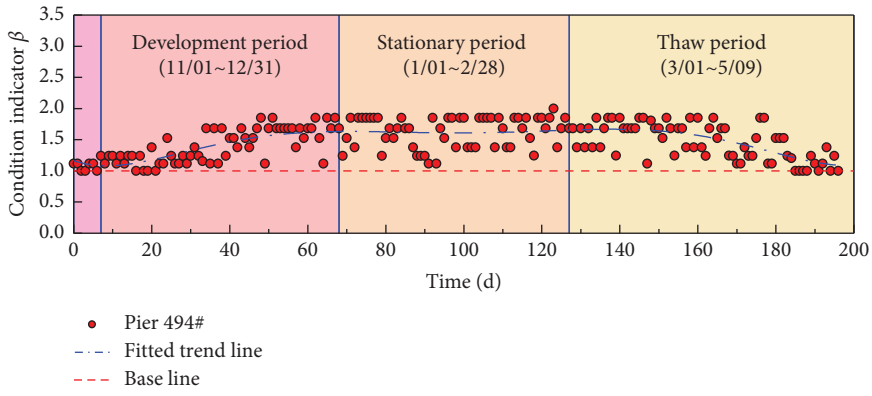

Figure 23: The identified condition indicator β of pier 494# using LMF.

passing train was uploaded to the cloud monitoring system through a 4G communication card and GPS antenna. The subsoil of the bridge site consists of three layers: (1) fine sand and silty clay (0~10.700 m); (2) medium sand and gravel (10.700~21.063 m); and (3) mudstone and sandstone interbedded (21.063 m~pile bottom). The results of the investigation of the in-situ geological environment are presented in Table 7, and the equivalent stiffnesses at the pier bottom can be determined by [26] as presented in Table 8.

Currently, the Chinese code applicable to rating the operational performance of existing HSR bridge substructures is code [43], which prescribes the normal value of lateral amplitude at the pier top when multiple units pass through the bridge, as described in Table 9. The normal values in the table are applicable to solid piers, hollow piers, and double cylindrical piers of double line bridges. H_p is the total height of the pier, and B is lateral average width of pier shaft. It is noted that the code stipulates that when the lateral

forced vibration frequency is close to the lateral natural frequency of the pier-beam system, the maximum transverse amplitude of the pier top should not be greater than twice the normal value.

According to statistics, approximately 82~86 trains pass through the bridge monitoring site every day. Figure 19 shows the daily statistical diagram of amplitude at the top of pier 494# on October 25th. Apart from the high level of dispersion of the data, it is evident that the lateral forced vibration frequencies of over half of the trains closely resemble the lateral natural frequency of the pier-beam system, causing the amplitude of the pier top to surpass the normal value. At this point, the operational performance of the bridge substructure should be assessed utilizing twice the normal value specified by the code. The average value of the maximum amplitude at the pier top during the daily passage of all trains on pier 494# during the entire monitoring period has been plotted as shown in Figure 20. It can be seen that all statistical values fall below twice the normal value, indicating that the substructure is currently operating well. However, the amplitude results show significant fluctuations, high dispersion, and no notable trend of change throughout the entire monitoring period. This is because the waveform and amplitude of bridge piers under train excitation vary with different train speeds, types, axle loads, and track irregularities. In practical applications, analysis can only be based on a certain probability of exceedance. Therefore, it is difficult to use amplitude indicators to reflect the effect of freeze-thaw on the structure in the evaluation of the service performance of railway bridge piers in severe cold regions.

The evolution diagram of the lateral natural frequencies of pier 494# extracted by RD-FFT during the entire monitoring period is shown in Figure 21. It can be seen from the figure that the identification results are relatively concentrated, and the changes of structural frequency have a notable evolutionary pattern throughout the entire monitoring period, which is consistent with the temperature data changes recorded in Figure 22, and the evolution process can be generally divided into three stages. As the average temperature gradually decreases during the freeze-thaw development period, the soil layer begins to freeze and the foundation stiffness continues to increase, ultimately leading to an increase in the structural natural frequency. As the frozen soil layer completed freezing, the natural frequency of the structure entered a stationary period, which approximately lasts from early January to the end of February. Since the beginning of March, the seasonal frozen soil layer has been gradually melting, causing a decrease in the structural stiffness as the average temperature rises, and the lateral fundamental frequency of the substructure has been gradually returning to its presoil-freezing level.

The results of quantitative system identification using LMF are depicted in Figure 23. As observed, the foundation condition indices during the monitoring period are larger than 1.0, indicating that the pier 494# is in good health condition, which agrees well with the amplitude-based evaluation results. The proposed method possesses good capability in tracking the operational performance and quantitatively evaluating the HSR bridge substructures and offers a novel solution for condition monitoring and quantitative evaluation of railway bridge substructures by utilizing daily operational train-induced vibration responses and only one transducer installed on the pier top.

6. Conclusions

The current codes implemented in China mainly rely on the amplitude of the pier top to evaluate and monitor the health status of the railway bridge substructures. The amplitude-based indicators can only be used to qualitatively determine the existence of damage, and they exhibit significant dispersion and randomness. This paper presents a novel methodology for quantitative evaluating railway bridge substructures online by utilizing operational train-induced responses and a single vibration sensor installed on the pier top. A flexible-base Timoshenko beam model that is capable of interpreting the traverse dynamics of both shallow foundation and pile foundation is derived theoretically. The RD-FFT is employed to extract the modal parameters of the bridge substructure, and the spring stiffnesses at pier bottom are constructed as an indicator. The condition indicator is updated by the LMF algorithm to quantitatively reflect the status of bridge foundation. Based on the preformed numerical and experimental investigations, the main conclusions can be drawn as follows:

(1) The proposed flexible-base Timoshenko beam model exhibits greater computational accuracy than the Euler–Bernoulli beam model, especially for low piers, making it suitable for the modal analysis and quantitative evaluation of bridge substructures.

(2) The extracted modal frequency of bridge substructures using the RD-FFT and train-induced vibrations shows good agreement with those identified by IVTM and SSI, thus validating the proposed approach's effectiveness and good antinoise ability.

(3) The LMF algorithm exhibits better identification accuracy compared to TRR, requiring less computation time to achieve satisfactory identification accuracy with an error of less than ±1%.

(4) The proposed method shows good performance in quantitatively monitoring the service condition of the HSR bridge substructures under freeze-thaw cycles, which also has great potential to characterize the evolutionary process of the substructure in other application scenarios.

Ongoing efforts involve the development of more sophisticated analytical models and modal identification algorithms aimed at characterizing and extracting the high-order dynamic signatures of the bridge substructure.

Furthermore, a spatial comprehensive condition assessment by merging the three-dimensional structural responses and considering the influence of environmental factors will also be conducted in our future study.

Data Availability

The experimental data used to support the findings of this study are available from the corresponding author upon request.

Conflicts of Interest

The authors declare that there are no conflicts of interest regarding the publication of this paper.

Acknowledgments

This study was sponsored by the National Natural Science Foundation of China (Grant no. 52178100) and the Fundamental Research Funds for the Central Universities (Grant no. 2022YJS070). The financial aids are gratefully acknowledged.

References

[1] B. Bozyigit and S. Acikgoz, "Dynamic amplification in masonry arch railway bridges," *Structures*, vol. 45, pp. 1717–1728, 2022.

[2] Q. Mao, M. Mazzotti, M. Furkan, A. Hicks, I. Bartoli, and E. Aktan, "Characterization of bridge substructures explored by leveraging structural identification of a scaled bridge model," *Engineering Structures*, vol. 246, Article ID 112953, 2021.

[3] E. Ghorbani, D. Svecova, D. J. Thomson, and Y.-J. Cha, "Bridge pier scour level quantification based on output-only Kalman filtering," *Structural Health Monitoring*, vol. 21, no. 5, pp. 2116–2135, 2022.

[4] M. S. Hossain, M. S. Khan, J. Hossain, G. Kibria, and T. Taufiq, "Evaluation of unknown foundation depth using different NDT methods," *Journal of Performance of Constructed Facilities*, vol. 27, no. 2, pp. 209–214, 2013.

[5] B. Chen, Y. Yang, J. Zhou, Y. Zhuang, and M. McFarland, "Damage detection of underwater foundation of a Chinese ancient stone arch bridge via sonar-based techniques," *Measurement*, vol. 169, Article ID 108283, 2021.

[6] S. Rashidyan, T. Ng, and A. Maji, "Practical aspects of nondestructive induction field testing in determining the depth of steel and reinforced concrete foundations," *Journal of Nondestructive Evaluation*, vol. 38, no. 1, p. 19, 2019.

[7] G. A. F. Cardoso and B. D. C. F. L. Lopes, "ERT feasibility study to assess unknown bridge foundation depth," *Journal of Bridge Engineering*, vol. 27, no. 7, Article ID 06022002, 2022.

[8] X. Kong, S. C. M. Ho, G. B. Song, and C. S. Cai, "Scour monitoring system using fiber bragg grating sensors and water-swellable polymers," *Journal of Bridge Engineering*, vol. 22, no. 7, Article ID 04017029, 2017.

[9] W. K. Liu, W. S. Zhou, and H. Li, "Bridge scour estimation using unconstrained distributed fiber optic sensors," *Journal of Civil Structural Health Monitoring*, vol. 12, no. 4, pp. 775–784, 2022.

[10] S. H. Jiang, Q. L. Wang, W. H. Sun, and Y. Tan, "Bridge scour monitoring using smart magnetic rock," *Measurement*, vol. 205, Article ID 112175, 2022.

[11] Y. Z. Chen, F. J. Tang, Z. C. Li, G. D. Chen, and Y. Tang, "Bridge scour monitoring using smart rocks based on magnetic field interference," *Smart Materials and Structures*, vol. 27, no. 8, Article ID 085012, 2018.

[12] Z. C. Li, F. J. Tang, Y. Z. Chen, X. Y. Hu, G. D. Chen, and Y. Tang, "Field experiment and numerical verification of the local scour depth of bridge pier with two smart rocks," *Engineering Structures*, vol. 249, Article ID 113345, 2021.

[13] M. L. Funderburk, Y. Park, A. Netchaev, and K. J. Loh, "Piezoelectric rod sensors for scour detection and vortex-induced vibration monitoring," *Structural Health Monitoring*, vol. 21, no. 3, pp. 1031–1045, 2021.

[14] B. Bozyigit and S. Acikgoz, "Determination of free vibration properties of masonry arch bridges using the dynamic stiffness method," *Engineering Structures*, vol. 250, Article ID 113417, 2022.

[15] L. J. Prendergast, D. Hester, K. Gavin, and J. J. O'Sullivan, "An investigation of the changes in the natural frequency of a pile affected by scour," *Journal of Sound and Vibration*, vol. 332, no. 25, pp. 6685–6702, 2013.

[16] L. J. Prendergast, D. Hester, and K. Gavin, "Determining the presence of scour around bridge foundations using vehicle-induced vibrations," *Journal of Bridge Engineering*, vol. 21, no. 10, Article ID 04016065, 2016.

[17] A. Elsaid and R. Seracino, "Rapid assessment of foundation scour using the dynamic features of bridge superstructure," *Construction and Building Materials*, vol. 50, pp. 42–49, 2014.

[18] K. W. Liao, M. Y. Cheng, Y.-F. Chiu, and J.-H. Lee, "Preliminary bridge health evaluation using the pier vibration frequency," *Construction and Building Materials*, vol. 102, pp. 552–563, 2016.

[19] A. Malekjafarian, C. W. Kim, E. J. Obrien, L. J. Prendergast, P. C. Fitzgerald, and S. Nakajima, "Experimental demonstration of a mode shape-based scour-monitoring method for multi-span bridges with shallow foundations," *Journal of Bridge Engineering*, vol. 25, no. 8, Article ID 04020050, 2020.

[20] C. C. Chen, W. H. Wu, F. Shih, and S. W. Wang, "Scour evaluation for foundation of a cable-stayed bridge based on ambient vibration measurements of superstructure," *NDT&E International*, vol. 66, no. 0, pp. 16–27, 2014.

[21] N. T. Davis and M. Sanayei, "Foundation identification using dynamic strain and acceleration measurements," *Engineering Structures*, vol. 208, Article ID 109811, 2020.

[22] Q. Mao, M. Mazzotti, J. DeVitis et al., "Structural condition assessment of a bridge pier: a case study using experimental modal analysis and finite element model updating," *Structural Control and Health Monitoring*, vol. 26, no. 1, Article ID e2273, 2019.

[23] S. Carbonari, F. Dezi, D. Arezzo, and F. Gara, "A methodology for the identification of physical parameters of soil-foundation-bridge pier systems from identified state-space models," *Engineering Structures*, vol. 255, Article ID 113944, 2022.

[24] J. W. Zhan, C. Wang, Y. Z. Yan, L. Deng, W. J. Zhu, and J. L. Liu, "Modal analysis and condition evaluation of substructures for simply supported high-speed railway bridge based on a simplified model," *Journal of Bridge Engineering*, vol. 27, no. 8, Article ID 04022058, 2022.

[25] J. W. Zhan, Y. J. Wang, F. Zhang, Y. H. An, and K. Liu, "Scour depth evaluation of highway bridge piers using vibration measurements and finite element model updating," *Engineering Structures*, vol. 253, Article ID 113815, 2022.

[26] MOR (Ministry of Railways), *Code for Design on Subsoil and Foundation of Railway Bridge and Culvert. TB10093-2017*, China Railway Publishing House, Beijing, 2017.

[27] H. Xia, N. Zhang, and W. W. Guo, *Dynamic Interaction of Train-Bridge Systems in High-Speed Railways*, Springer, Berlin, Heidelberg, 2018.

[28] J. W. Zhan, J. J. You, X. Kong, and N. Zhang, "An indirect bridge frequency identification method using dynamic responses of high-speed railway vehicles," *Engineering Structures*, vol. 243, Article ID 112694, 2021.

[29] C. Wang, J. W. Zhan, Y. J. Wang, F. Zhang, and D. J. Pan, "A drive-by methodology for rapid inspection of HSR bridge substructures using dynamic responses of passing marshaling trains," *International Journal of Structural Stability and Dynamics*, vol. 24, no. 06, Article ID 2450068, 2023.

[30] B. Bozyigit, "Dynamic response of damaged rigid-frame bridges subjected to moving loads using analytical based formulations," *Engineering Computations*, vol. 40, no. 4, pp. 793–822, 2023.

[31] B. Bozyigit, I. Bozyigit, and L. J. Prendergast, "Analytical approach for seismic analysis of onshore wind turbines considering soil-structure interaction," *Structures*, vol. 51, pp. 226–241, 2023.

[32] J. C. Bruch and T. P. Mitchell, "Vibrations of a mass-loaded clamped-free Timoshenko beam," *Journal of Sound and Vibration*, vol. 114, no. 2, pp. 341–345, 1987.

[33] W. H. Liu, "Comments on "Vibrations of a mass-loaded clamped-free Timoshenko beam"," *Journal of Sound and Vibration*, vol. 129, no. 2, pp. 343-344, 1989.

[34] S. H. Farghaly, "On comments on "vibration of a mass-loaded clamped-free Timoshenko beam"," *Journal of Sound and Vibration*, vol. 164, no. 3, pp. 549–552, 1993.

[35] Matlab, *MATLAB Version R2021a*, The Mathworks, Inc, Natick, MA, USA, 2021.

[36] H. A. Cole, "Failure detection of a space shuttle wing by random decrement," *Technical Report NASA TMX-62041*, 1971.

[37] J. K. Vandiver, A. B. Dunwoody, R. B. Campbell, and M. F. Cook, "A mathematical basis for the random decrement vibration signature analysis technique," *Journal of Mechanical Design*, vol. 104, no. 2, pp. 307–313, 1982.

[38] M. Balda, "LMFnlsq2, MATLAB central file exchange," 2023, https://www.mathworks.com/matlabcentral/fileexchange/39564-lmfnlsq2.

[39] W. Guo, Z. Y. Bai, X. B. Wang et al., "A combination strategy of hollow-closed-wall in-filled trench and elastic bearing for reducing environmental vibration induced by high-speed train," *Soil Dynamics and Earthquake Engineering*, vol. 133, Article ID 106136, 2020.

[40] G. H. Golub and R. Underwood, "The block Lanczos method for computing eigenvalues," *Mathematical Software*, pp. 361–377, 1977.

[41] J. W. Zhan, H. Xia, and J. B. Yao, "Damage evaluation of bridge foundations considering subsoil properties," *In Environmental Vibrations: Prediction, Monitoring, Mitigation and Evaluation*, pp. 271–277, Taylor and Francis, London, 2005.

[42] E. Reynders, R. Pintelon, and G. De Roeck, "Uncertainty bounds on modal parameters obtained from stochastic subspace identification," *Mechanical Systems and Signal Processing*, vol. 22, no. 4, pp. 948–969, 2008.

[43] CRC (China Railway Corporation), *Code for Rating Operational Performance of Existing High-Speed Railway Bridges (To Try Out). TG/GW 209-2014*, China Railway Publishing House, Beijing, 2014.